

Geometric statistics with subspace structure preservation for SPD matrices [★]

Cyrus Mostajeran^{*} Nathaël Da Costa^{**}
Graham Van Goffrier^{***} Rodolphe Sepulchre^{****}

^{*} *School of Physical and Mathematical Sciences, Nanyang Technological University, Singapore (e-mail: cyrussam.mostajeran@ntu.edu.sg)*

^{**} *Tübingen AI Center, University of Tübingen, Tübingen, Germany (e-mail: nathael.da-costa@uni-tuebingen.de)*

^{***} *Department of Physics and Astronomy, University College London, London, United Kingdom (e-mail: vangoffrier@gmail.com)*

^{****} *Department of Engineering, University of Cambridge, United Kingdom & Department of Electrial Engineering, KU Leuven, Belgium (e-mail:rs771@cam.ac.uk)*

Abstract: We present a geometric framework for the processing of SPD-valued data that preserves subspace structures and is based on the efficient computation of extreme generalized eigenvalues. This is achieved through the use of the Thompson geometry of the semidefinite cone. We explore a particular geodesic space structure in detail and establish several properties associated with it. Finally, we review a novel inductive mean of SPD matrices based on this geometry.

Keywords: convex cones, differential geometry, geodesics, geometric statistics, positive definite matrices, matrix means, Thompson metric

1. INTRODUCTION

The space of $n \times n$ symmetric positive definite (SPD) matrices \mathbb{S}_{++}^n forms the interior of the convex cone of positive semidefinite matrices in the vector space of $n \times n$ symmetric matrices. Several Riemannian geometries on SPD matrices have been proposed and used effectively in a variety of applications in computer vision, medical data analysis, machine learning, and optimization. In particular, the affine-invariant Riemannian metric—so-called because it is invariant to affine transformations of the underlying spacial coordinates—has received considerable attention in recent years and applied successfully to problems such as EEG signal processing in BCI where it has been shown to be superior to classical techniques based on feature vector classification (Barachant et al., 2012).

The affine-invariant Riemannian metric endows the space of SPD matrices of a given dimension with the structure of a Riemannian symmetric space and a metric space of non-positive curvature (Said et al., 2017). Computing standard geometric objects such as distances, geodesics, Riemannian exponentials and logarithms in this geometry often amounts to the computation of the generalized eigenspectrum of a pair of SPD matrices, which typically

means a significant increase in computational complexity, particularly for larger matrices. In particular, the affine-invariant Riemannian structure induces the distance function $d_R : \mathbb{S}_{++}^n \times \mathbb{S}_{++}^n \rightarrow \mathbb{R}$

$$d_R(X, Y) = \left(\sum_{i=1}^n \log^2 \lambda_i(YX^{-1}) \right)^{1/2}, \quad (1)$$

where $\lambda_i(YX^{-1}) = \lambda_i(X^{-1/2}YX^{-1/2})$ denote the n real and positive eigenvalues of YX^{-1} . (1) satisfies two key symmetries that contribute to its success in a variety of applications: (i) affine-invariance, i.e., invariance under congruence transformations: $d_R(X, Y) = d_R(AXA^T, AYA^T)$ for any invertible matrix $A \in \text{GL}(n, \mathbb{R})$, where A^T denotes the transpose of A , and (ii) inversion-invariance, whereby $d_R(X, Y) = d_R(X^{-1}, Y^{-1})$.

The metric (1) also provides a way of defining the mean of a collection of N SPD matrices $\{Y_i\}$ as the Riemannian barycentre, i.e. as

$$\operatorname{argmin}_X \sum_{i=1}^N d_R(X, Y_i)^2, \quad (2)$$

which is known to exist and be unique in this geometry (Afsari, 2011).

While the Riemannian barycentre (2) has been employed effectively in numerous applications, it suffers from several drawbacks in specific contexts. Firstly, its computation can be costly for very large matrices. Secondly, it typically corrupts any sparsity or subspace structure inherent in the matrices $\{Y_i\}$, which may be an issue if such structures are of relevance to the underlying application. In this

[★] C.M. was supported by a Presidential Postdoctoral Fellowship at Nanyang Technological University (NTU Singapore) and an Early Career Research Fellowship at the University of Cambridge. G.V.G. was supported by the UCL Centre for Doctoral Training in Data Intensive Science funded by STFC, and by an Overseas Research Scholarship from UCL. The research leading to these results has also received funding from the European Research Council under the Advanced ERC Grant Agreement SpikyControl n.101054323.

paper, we will review how a statistical framework based on the Thompson geometry of the semidefinite cone can be used to achieve affine-invariance and define interpolations and means that preserve subspace structures. These have favourable computational properties for large matrices. We will also establish new properties of a distinguished geodesic of the Thompson metric. In Section 3.2, we consider the proximity of this distinguished Thompson geodesic to the affine-invariant Riemannian geodesic. We then establish in Section 3.3 general bounds for the distance between their associated midpoints.

2. HILBERT AND THOMPSON METRICS

A subset K of a vector space V is called a cone if it is convex, $\mu K \subseteq K$ for all $\mu \geq 0$, and $K \cap (-K) = \{0\}$. It is said to be a closed cone if it is a closed set in V with respect to the standard topology. A cone K in a vector space V induces a partial ordering on V given by $x \leq y$ if and only if $y - x \in K$, and this partial ordering can be used to define the Hilbert projective metric and Thompson metric on K (Thompson, 1963).

In the case of the positive semidefinite cone, we find that for strictly positive definite matrices $X, Y \succ 0$, the Hilbert and Thompson metrics take the forms

$$d_H(X, Y) = \log \left(\frac{\lambda_M(YX^{-1})}{\lambda_m(YX^{-1})} \right) \quad (3)$$

and

$$d_T(X, Y) = \log \left(\max\{\lambda_M(YX^{-1}), 1/\lambda_m(YX^{-1})\} \right), \quad (4)$$

respectively, where $\lambda_M(A)$ and $\lambda_m(A)$ denote the maximum and minimum eigenvalues of the matrix A . Note that both of these metrics satisfy affine-invariance and inversion-invariance. Moreover, both can be computed using extreme generalized eigenvalues (Mostajeran et al., 2020; Van Goffrier et al., 2021), which can be accessed efficiently using techniques such as Krylov subspace methods based on matrix-vector products. Finally, we note that the Thompson metric can equivalently be expressed as

$$\begin{aligned} d_T(X, Y) &= \max_{1 \leq i \leq n} |\log \lambda_i(YX^{-1})| \\ &= \max\{\log \lambda_M(YX^{-1}), \log \lambda_m(XY^{-1})\}. \end{aligned}$$

3. GEODESICS

If (M, d) is a metric space, a map $\gamma : [0, 1] \rightarrow M$ is said to be a geodesic path from $x_0 = \gamma(0)$ to $x_1 = \gamma(1)$ if $d(\gamma(s), \gamma(t)) = (t - s)d(x_0, x_1)$, whenever $0 \leq s < t \leq 1$. The image of a geodesic path is called a geodesic, and a metric space is said to be a geodesic space if there exists a geodesic path joining any two points. The curve $\gamma : [0, 1] \rightarrow \mathbb{S}_{++}^n$ defined by

$$\gamma(t) = X \#_t Y := X^{1/2} (X^{-1/2} Y X^{-1/2})^t X^{1/2} \quad (5)$$

is a geodesic path from X to Y for both the affine-invariant Riemannian metric and the Thompson metric in \mathbb{S}_{++}^n . In the Riemannian case, the corresponding geodesic is the unique geodesic connecting X to Y . However, in the Thompson geometry, there is typically a family of geodesics that generally consists of an infinite number of curves connecting a pair of points in \mathbb{S}_{++}^n (Nussbaum, 1994).

We will use one particular geodesic in (\mathbb{S}_{++}^n, d_T) from X to Y that has particularly attractive properties. This geodesic will be denoted by $X *_t Y$ and is given by

$$X *_t Y = \left(\frac{\lambda_M^t - \lambda_m^t}{\lambda_M - \lambda_m} \right) Y + \left(\frac{\lambda_M \lambda_m^t - \lambda_m \lambda_M^t}{\lambda_M - \lambda_m} \right) X \quad (6)$$

if $\lambda_M \neq \lambda_m$, and $X *_t Y = \lambda_m^t X$ otherwise. Note that $X *_t Y$ reduces to a linear combination of X and Y with coefficients that are nonlinear functions of the extreme generalized eigenvalues of (X, Y) and t . Furthermore, this geodesic satisfies the following joint homogeneity property for any $t \in \mathbb{R}$ and pair of positive scalars μ_1 and μ_2 :

$$(\mu_1 X_1) *_t (\mu_2 X_2) = \mu_1^{1-t} \mu_2^t (X_1 *_t X_2)$$

Finally, we note that if $X, Y \in \mathbb{S}_{++}^2$, then $X \#_t Y = X *_t Y$ for all $t \in [0, 1]$. That is, the $*_t$ Thompson geodesic coincides with the affine-invariant Riemannian geodesic in the case of 2×2 matrices.

3.1 Subspace structure preservation

Since $X *_t Y$ is a linear combination of X and Y for any $t \in \mathbb{R}$, it lies in the linear span of X and Y , and thus preserves any subspace structure that is common to X and Y . For example, if X and Y are banded, Toeplitz, or Henkel matrices, then these structures are preserved at every point along the geodesic $X *_t Y$. This is in contrast to the Riemannian geodesic (5), which generally corrupts such structures. A further consequence of the preservation of subspace structures by the $*_t$ Thompson geodesic is that it preserves sparsity. That is, if X and Y are sparse SPD matrices, then $X *_t Y$ is sparse for every $t \in \mathbb{R}$. In contrast, the Riemannian geodesic $X \#_t Y$, whose construction involves computing matrix square roots, matrix products, and matrix inverses, does not preserve sparsity. Thus, the use of Riemannian interpolation to process large sparse SPD matrices may be problematic. For instance, kernel matrices in machine learning are often built as sparse matrices to facilitate the analysis of large datasets. Applying the standard affine-invariant Riemannian geometry to process such SPD matrices will typically corrupt the sparse structure, potentially resulting in intractable computations.

3.2 Determinants along geodesics

Here we consider the evolution of determinants along various interpolations of SPD matrices, including Euclidean, Riemannian, and Thompson geodesics. An application in which the evolution of determinants along interpolations is of practical significance is diffusion tensor imaging (DTI), which is an imaging modality used to produce non-invasive reconstructions of brain tissue connectivity. DTI is based on the assumption that the motion of water molecules in each voxel of the image is well approximated by Brownian motion. This Brownian motion is characterized by an SPD matrix, called the diffusion tensor (Basser et al., 1994). Interpolating diffusion tensors is a basic operation in many data processing algorithms in DTI. It has been well documented that Euclidean interpolation and averaging of tensors generally results in a tensor swelling effect (Penec et al., 2006) where the determinant of the Euclidean average of SPD matrices is often larger than the determinant of the original SPD matrices. This phenomenon is

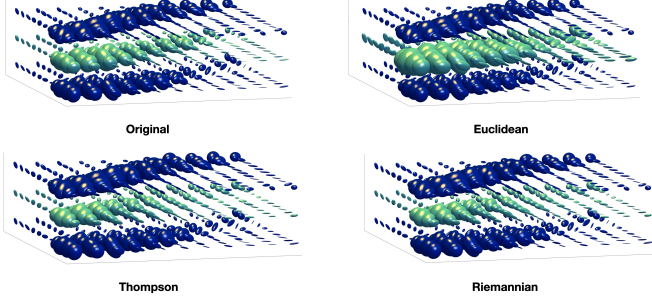


Fig. 1. Reconstructions of the middle layer of an image consisting of three layers of ellipsoids representing diffusion tensors using Euclidean, Riemannian, and Thompson geodesic interpolations. The Euclidean interpolation exhibits an undesirable swelling effect. The Riemannian and Thompson interpolations generate similar results and are more faithful to the original data.

problematic as the determinant of the diffusion tensor is a measure of the dispersion of the local diffusion process, whose increase upon averaging is physically unrealistic. To overcome this difficulty, the affine-invariant and Log-Euclidean Riemannian geometries are often used in data processing tasks in DTI such as interpolation and regularization (Arsigny et al., 2006; Pennec et al., 2006). In either of these Riemannian geometries, the swelling effect is eliminated and the determinants along the geodesics between two SPD matrices with the same determinant are constant. Indeed, for $X, Y \in \mathbb{S}_{++}^n$, we have $\det(X \#_t Y) = \det(X^{1/2}(X^{-1/2}YX^{-1/2})^t X^{1/2}) = (\det X)^{1-t}(\det Y)^t$. In particular,

$$\det(X \#_{1/2} Y) = \sqrt{\det(XY)}.$$

Thus, if $\det X = \det Y$, then $\det(X \#_t Y) = \det X = \det Y$ for all $t \in \mathbb{R}$. More generally, we see that the logarithm of the determinant interpolates linearly along the affine-invariant Riemannian geodesics.

These observations raise the question of how determinants evolve along the $\#_t$ Thompson geodesics. In Figure 1, we compare interpolations using three different geodesics with real data extracted from Alexander et al. (2006) in the context of DTI. Each image depicts three layers of ellipsoids corresponding to positive definite matrices. The middle layer of the original image consisting of real data was removed and reconstructed using Euclidean, Riemannian, and Thompson interpolations of data at voxels in the top and bottom layers. We observe that in the case of 3×3 matrices, the Riemannian and Thompson interpolations produce very similar reconstructions. The swelling effect in the case of the Euclidean interpolation is also clearly visible.

Further simulations suggest that in contrast to the Euclidean case, we seem to encounter a ‘shrinkage phenomenon’ when using the $\#_t$ Thompson geodesics, whereby determinants along the geodesic between two SPD matrices with the same determinant are reduced in value. While this effect appears modest in low dimensions, it can become quite dramatic in higher dimensions as seen in Figure 2. In the following proposition, we provide mathematical explanations for these observations and precisely

characterize the circumstances under which the shrinkage phenomenon is not present along interpolations of a pair of SPD matrices.

Proposition 1. Let $X, Y \in \mathbb{S}_{++}^n$ and λ_i denote the eigenvalues of YX^{-1} . Then

$$\begin{aligned} \det\left(\frac{X+Y}{2}\right) &= \sqrt{\det(XY)} \prod_{i=1}^n \left(\frac{\sqrt{\lambda_i} + \frac{1}{\sqrt{\lambda_i}}}{2}\right) \geq \sqrt{\det(XY)} \end{aligned} \quad (7)$$

where equality holds if and only if $X = Y$. Furthermore,

$$\begin{aligned} \det(X \#_{1/2} Y) &= \sqrt{\det(XY)} \prod_{i=1}^n \left[\frac{1}{\sqrt{\lambda_M} + \sqrt{\lambda_m}} \left(\sqrt{\lambda_i} + \frac{\sqrt{\lambda_M \lambda_m}}{\sqrt{\lambda_i}}\right)\right] \\ &\leq \sqrt{\det(XY)} \end{aligned} \quad (8)$$

where equality holds if and only if $\lambda_i \in \{\lambda_m, \lambda_M\}$ for $i = 1, \dots, n$, where λ_M and λ_m denote the maximum and minimum eigenvalues of YX^{-1} , respectively.

Proof. $X^{-1/2}YX^{-1/2}$ admits a diagonalization as QDQ^T , where Q is an orthogonal matrix and $D = \text{diag}(\lambda_1, \dots, \lambda_n)$. We have

$$\begin{aligned} \det\left(\frac{X+Y}{2}\right) &= \det\left(X^{1/2} \frac{(I + X^{-1/2}YX^{-1/2})}{2} X^{1/2}\right) \\ &= \det(X) \det\left(\frac{I + QDQ^T}{2}\right) \\ &= \det(X) \det\left(\frac{I + D}{2}\right) \\ &= \det(X) \det(D^{1/2}) \det\left(\frac{D^{1/2} + D^{-1/2}}{2}\right) \\ &= \sqrt{\det(XY)} \det\left(\frac{D^{1/2} + D^{-1/2}}{2}\right) \\ &= \sqrt{\det(XY)} \prod_{i=1}^n \left(\frac{\sqrt{\lambda_i} + \frac{1}{\sqrt{\lambda_i}}}{2}\right), \end{aligned}$$

where we have repeatedly used the fact that $\det(AB) = \det(A)\det(B)$ for square $n \times n$ matrices A and B . The inequality (7) now follows by noting the identity

$$\frac{1}{2} \left(\sqrt{\lambda_i} + \frac{1}{\sqrt{\lambda_i}}\right) \geq 1,$$

where equality holds if and only if $\lambda_i = 1$. Thus, each term in the product in (7) results in a scaling of the geometric mean $\sqrt{\det(XY)}$ by a factor greater than or equal to 1, which contributes to the swelling effect. For the swelling effect to completely disappear, we would need $\lambda_i = 1$ for each i , which is only possible in the trivial case when $X = Y$.

We now apply a similar analysis to $\det(X \#_{1/2} Y)$ to find

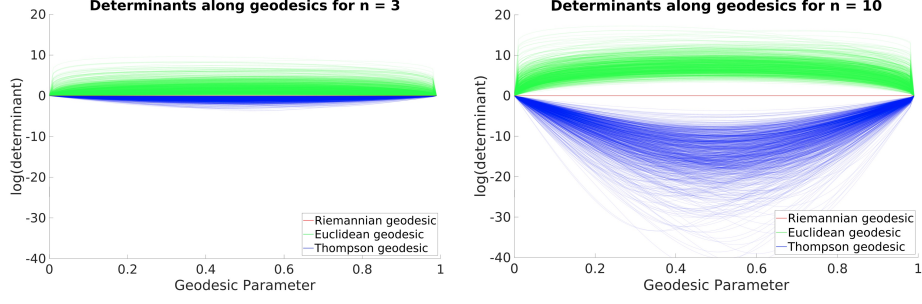


Fig. 2. Plots of the logarithm of the determinants along Euclidean, Riemannian, and Thompson geodesics connecting 1,000 pairs of randomly generated $n \times n$ SPD matrices of unit determinant for $n = 3$ and $n = 10$. We observe that the determinants along the Riemannian geodesics are constant and equal to one as expected. The determinants along Euclidean interpolations exhibit swelling, whereas an opposite shrinkage effect is observed for interpolations along the Thompson geodesics. Both of these effects are magnified in higher dimensions.

$$\begin{aligned}
& \det(X \#_{1/2} Y) \\
&= \det\left(\frac{1}{\sqrt{\lambda_M} + \sqrt{\lambda_m}}(Y + \sqrt{\lambda_M \lambda_m} X)\right) \\
&= \det(X) \det\left(\frac{1}{\sqrt{\lambda_M} + \sqrt{\lambda_m}}(X^{-1/2} Y X^{-1/2} + \sqrt{\lambda_M \lambda_m} I)\right) \\
&= \det(X) \det\left(\frac{1}{\sqrt{\lambda_M} + \sqrt{\lambda_m}}(Q D Q^T + \sqrt{\lambda_M \lambda_m} I)\right) \\
&= \det(X) \det\left(\frac{1}{\sqrt{\lambda_M} + \sqrt{\lambda_m}}(D + \sqrt{\lambda_M \lambda_m} I)\right) \\
&= \sqrt{\det(XY)} \det\left(\frac{1}{\sqrt{\lambda_M} + \sqrt{\lambda_m}}(D^{1/2} + \sqrt{\lambda_M \lambda_m} D^{-1/2})\right) \\
&= \sqrt{\det(XY)} \prod_{i=1}^n \left[\frac{1}{\sqrt{\lambda_M} + \sqrt{\lambda_m}} \left(\sqrt{\lambda_i} + \frac{\sqrt{\lambda_M \lambda_m}}{\sqrt{\lambda_i}}\right)\right].
\end{aligned}$$

Now, the inequality (8) follows from

$$\begin{aligned}
& \frac{1}{\sqrt{\lambda_M} + \sqrt{\lambda_m}} \left(\sqrt{\lambda_i} + \frac{\sqrt{\lambda_M \lambda_m}}{\sqrt{\lambda_i}}\right) - 1 \\
&= \frac{(\sqrt{\lambda_M} - \sqrt{\lambda_i})(\sqrt{\lambda_m} - \sqrt{\lambda_i})}{\sqrt{\lambda_i}(\sqrt{\lambda_M} + \sqrt{\lambda_m})} \leq 0,
\end{aligned}$$

for each $i = 1, \dots, n$, which holds since $\lambda_m \leq \lambda_i \leq \lambda_M$. Moreover, we see that equality holds if and only if $\lambda_i = \lambda_m$ or $\lambda_i = \lambda_M$ for all i . Thus, we see that each term in the product results in a scaling of the geometric mean $\sqrt{\det(XY)}$ by a factor less than or equal to 1, which contributes to the shrinkage effect. As the dimension increases, we expect this product to include more and more factors smaller than 1, which explains the intensification of this shrinkage effect with the dimension n . The shrinkage is fully eliminated if and only if each of the factors in the product is equal to 1, which occurs precisely if $\lambda_i \in \{\lambda_m, \lambda_M\}$ for all $i = 1, \dots, n$.

3.3 Distances between geodesic mid-points

We have seen that the affine-invariant Riemannian and $\#_t$ Thompson geodesics coincide in \mathbb{S}_{++}^2 . Moreover, simulations in \mathbb{S}_{++}^3 suggest that while the two geodesics no longer agree for 3×3 SPD matrices, they result in qualitatively similar interpolations. This raises the question of how close these two geodesics may be in higher dimensions. To investigate this, we consider the affine-invariant Riemannian distance between the midpoints of the two geodesics

connecting a pair of arbitrary SPD matrices X and Y . To simplify the notation, we denote the Riemannian and $\#_t$ Thompson geodesic midpoints by $X \# Y$ and $X * Y$, respectively.

Proposition 2. Let $X, Y \in \mathbb{S}_{++}^n$ and denote the eigenvalues of YX^{-1} by λ_i . Then,

$$\begin{aligned}
& d_R(X \# Y, X * Y) \\
&= \left[\sum_{i=1}^n \log^2 \left(\frac{1}{\sqrt{\lambda_M} + \sqrt{\lambda_m}} \left(\sqrt{\lambda_i} + \frac{\sqrt{\lambda_M \lambda_m}}{\sqrt{\lambda_i}} \right) \right) \right]^{1/2},
\end{aligned} \tag{9}$$

where $\lambda_m = \min_i \lambda_i$, and $\lambda_M = \max_i \lambda_i$. Furthermore,

$$0 \leq d_R(X \# Y, X * Y) \leq \sqrt{n-2} \log \left(\cosh \frac{d_T(X, Y)}{2} \right), \tag{10}$$

where $d_R(X \# Y, X * Y) = 0$ if and only if $\lambda_i \in \{\lambda_m, \lambda_M\}$ for $i = 1, \dots, n$, and the upper bound in (10) is attained if and only if $\lambda_m = 1/\lambda_M$ and $\lambda_i = 1$ for the remaining $n-2$ eigenvalues of YX^{-1} .

Proof. By affine-invariance of d_R , we have

$$\begin{aligned}
& d_R(X \# Y, X * Y) \\
&= d_R \left(X^{1/2} (X^{-1/2} Y X^{-1/2})^{1/2} X^{1/2}, \frac{Y + \sqrt{\lambda_M \lambda_m} X}{\sqrt{\lambda_M} + \sqrt{\lambda_m}} \right) \\
&= d_R \left((X^{-1/2} Y X^{-1/2})^{1/2}, \frac{X^{-1/2} Y X^{-1/2} + \sqrt{\lambda_M \lambda_m} I}{\sqrt{\lambda_M} + \sqrt{\lambda_m}} \right) \\
&= \left\| \log \left(\frac{1}{\sqrt{\lambda_M} + \sqrt{\lambda_m}} \left(\Sigma^{1/2} + \sqrt{\lambda_M \lambda_m} \Sigma^{-1/2} \right) \right) \right\|,
\end{aligned} \tag{11}$$

where $\Sigma = X^{-1/2} Y X^{-1/2}$ and $\|\cdot\|$ denotes the Frobenius norm. By noting that Σ admits a diagonalization $\Sigma = Q D Q^T$, where Q is an orthogonal matrix and $D = \text{diag}(\lambda_1, \dots, \lambda_n)$, and considering the eigenvalues of the matrix logarithm in (11), we arrive at (9).

It follows from (9) that $d_R(X \# Y, X * Y) = 0$ if and only if

$$\frac{1}{\sqrt{\lambda_M} + \sqrt{\lambda_m}} \left(\sqrt{\lambda_i} + \frac{\sqrt{\lambda_M \lambda_m}}{\sqrt{\lambda_i}} \right) = 1$$

for $i = 1, \dots, n$, which holds if and only if $(\sqrt{\lambda_i} - \sqrt{\lambda_M})(\sqrt{\lambda_i} - \sqrt{\lambda_m}) = 0$. That is, $d_R(X \# Y, X * Y) = 0$ if and only if $\lambda_i \in \{\lambda_m, \lambda_M\}$ for $i = 1, \dots, n$.

Now denote by r the Thompson distance $d_T(X, Y) = \max_i |\log \lambda_i|$ between X and Y . It follows that $\lambda_M = e^r$ or $\lambda_m = e^{-r}$. Suppose that $\lambda_M = e^r$ and note that (9) can be expressed as

$$d_R(X \# Y, X * Y) = \left(\sum_{i=1}^n \rho(\lambda_i) \right)^{1/2}, \quad (12)$$

where

$$\rho(x) = \log^2 \left(\frac{1}{\sqrt{\lambda_M} + \sqrt{\lambda_m}} \left(\sqrt{x} + \frac{\sqrt{\lambda_M \lambda_m}}{\sqrt{x}} \right) \right),$$

for $x \in [\lambda_m, \lambda_M]$. To establish the upper bound in (10), we seek to maximize (9) subject to the constraint that $e^{-r} \leq \lambda_m \leq \lambda_i \leq \lambda_M = e^r$. For a given λ_m , this is achieved by maximizing $\rho(\lambda_i)$ for every choice λ_i not corresponding to the extreme eigenvalues. ρ is a non-negative continuous function on $[\lambda_m, \lambda_M]$ that is smooth on (λ_m, λ_M) and satisfies $\rho'(x) = 0$ if and only if $x = \sqrt{\lambda_m \lambda_M}$. Since $\rho(\lambda_m) = \rho(\lambda_M) = 0$, it follows that (12) is maximized for a given λ_m and λ_M if and only if all remaining eigenvalues satisfy $\lambda_i = \sqrt{\lambda_m \lambda_M}$. For such a distribution of eigenvalues, (12) reduces to

$$d_R(X \# Y, X * Y) = \left((n-2) \log^2 \left(\frac{2e^{r/4} \lambda_m^{1/4}}{e^{r/2} + \lambda_m^{1/2}} \right) \right)^{1/2},$$

which in turn is maximized as a function of λ_m subject to the constraint $e^{-r} \leq \lambda_m \leq \lambda_M = e^r$ when $\lambda_m = e^{-r}$, at which point

$$\begin{aligned} d_R(X \# Y, X * Y) &= \left((n-2) \log^2 \left(\frac{2}{e^{r/2} + e^{-r/2}} \right) \right)^{1/2} \\ &= \sqrt{n-2} \log \left(\cosh \frac{r}{2} \right). \end{aligned}$$

Repeating the analysis by starting with the assumption that $\lambda_m = e^{-r}$ instead of $\lambda_M = e^r$ would yield the same conclusion. That is, the upper bound in (10) holds and is attained if and only if $\lambda_m = e^{-r}$, $\lambda_M = e^r$, and $\lambda_i = \sqrt{\lambda_m \lambda_M} = 1$ for the remaining $n-2$ eigenvalues of YX^{-1} , where $r = d_T(X, Y)$.

While we see that the bounds in (10) are attainable, it is generally unlikely that two SPD matrices X and Y will have the generalized eigenvalues required to attain these bounds. Indeed, the required distributions of generalized eigenvalues become increasingly unlikely as the dimension n grows. To develop a more practical sense of the typical values of the distance $d_R(X \# Y, X * Y)$, we can compute this distance for a large number of randomly generated SPD matrices. As (9) provides an expression for $d_R(X \# Y, X * Y)$ in terms of the eigenvalues of YX^{-1} , it allows us to efficiently simulate a large number of matrix distance computations by sampling vectors of generalized eigenvalues instead of generating a large number of pairs of SPD matrices and computing the corresponding generalized eigenvalues. Thus, we consider the ‘normalized’ distance function

$$\begin{aligned} f(\boldsymbol{\lambda}) &:= \frac{\sqrt{\sum_i \log^2 \left(\frac{1}{\sqrt{\lambda_M} + \sqrt{\lambda_m}} \left(\sqrt{\lambda_i} + \frac{\sqrt{\lambda_M \lambda_m}}{\sqrt{\lambda_i}} \right) \right)}}{\max_i |\log \lambda_i|} \\ &= \frac{d_R(X \# Y, X * Y)}{d_T(X, Y)} \end{aligned} \quad (13)$$

where f is a positive-valued function of $\boldsymbol{\lambda} = (\lambda_1, \dots, \lambda_n)$. The results in (3) were produced by generating 100,000 points $\boldsymbol{\lambda}$ for values of $r = \max_i |\log \lambda_i|$ from 0 to 100 and computing the corresponding $f(\boldsymbol{\lambda})$ in the cases $n = 4$ and $n = 20$. The solid blue curve above each plot indicates the corresponding upper bound as a function of r . We note that in either case most points concentrate away from the bounds and increasingly so in higher dimensions. By (10), we have

$$0 \leq f(\boldsymbol{\lambda}) \leq \sqrt{n-2} \frac{\log \left(\cosh \frac{r}{2} \right)}{r}. \quad (14)$$

4. INDUCTIVE MEAN

An important step in developing a computational framework for performing analysis and statistics on SPD-valued data using extreme generalized eigenvalues is to provide a suitable definition for the mean of a collection of k SPD matrices whose computation can be based primarily on finding a sequence of extreme generalized eigenvalues. Here, we review a result from Mostajeran et al. (2024) that provides an inductive algorithm based on Thompson geodesics that achieves this.

Algorithm 1: Generate inductive sequence of SPD matrices $(X_i)_{i \geq 1}$ from an initial point X_1 and the finite ordered set $\mathcal{P} = (Y_1, \dots, Y_k) \subset \mathbb{S}_{++}^n$

```

for  $i \geq 1$  do
  | Set  $j \equiv i \pmod k$  for  $1 \leq j \leq k$ .
  | Define  $X_{i+1} = X_i *_{\frac{1}{i+1}} Y_j$ .
end
return  $(X_1, X_2, X_3, \dots)$ .

```

Theorem 3. Let $(X_i)_{i \geq 1}$ denote any sequence generated by Algorithm 1. Then, $(X_i)_{i \geq 1}$ converges to a unique point X^* that is independent of the choice of initialization X_1 and lies in the linear span of $\{Y_1, \dots, Y_k\}$.

Thanks to Theorem 3, we have a well-defined inductive mean $M(Y_1, \dots, Y_k) = X^*$ of $\mathcal{P} = (Y_1, \dots, Y_k) \subset \mathbb{S}_{++}^n$. This mean is invariant to permutation of the Y_j and satisfies the following properties:

- (1) Affine-equivariance:

$$M(AY_1A^T, \dots, AY_kA^T) = AM(Y_1, \dots, Y_k)A^T$$

for any invertible matrix A .

- (2) Joint homogeneity:

$$M(c_1 Y_1, \dots, c_k Y_k) = (c_1 \cdots c_k)^{1/k} M(Y_1, \dots, Y_k)$$

for any $c_1, \dots, c_k > 0$.

See Mostajeran et al. (2024) for the proof of Theorem 3 and the above properties of the resulting inductive Thompson mean.

The subspace structure preservation property of the inductive mean leads to the following corollaries concerning sparsity preservation.

Corollary 4. (Sparsity preservation I). If $\{Y_1, \dots, Y_k\}$ is a set of SPD matrices with the same sparsity pattern (i.e., with non-zero elements restricted to a common set of entries), then $M(Y_1, \dots, Y_k)$ has the same sparsity pattern.

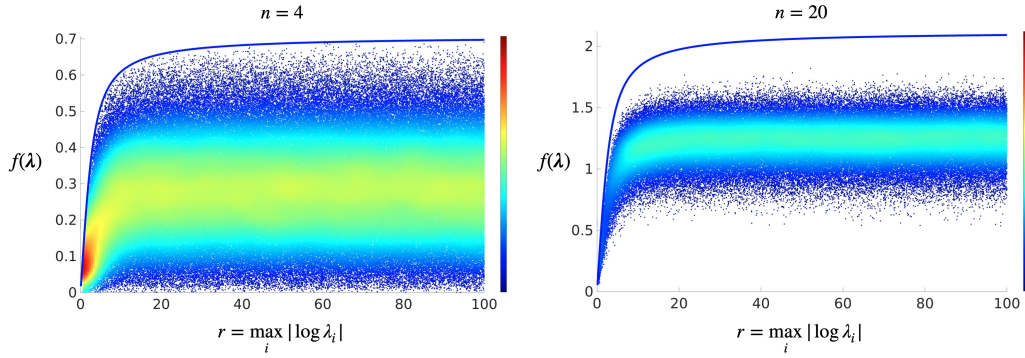


Fig. 3. Plots of $f(\boldsymbol{\lambda})$ (13) against $r = \max_i |\log \lambda_i|$ for 100,000 samples $\boldsymbol{\lambda} \in \mathbb{R}_+^n$ for $n = 4$ and $n = 20$. The solid blue curves represent the upper bounds of $f(\boldsymbol{\lambda})$ given in (14). The color scheme is used to indicate the density of plot points $(r, f(\boldsymbol{\lambda}))$.

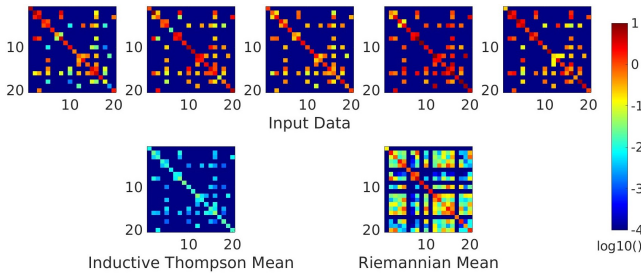


Fig. 4. The inductive Thompson mean and Riemannian mean for a set of 5 input data SPD matrices with the same sparsity pattern.

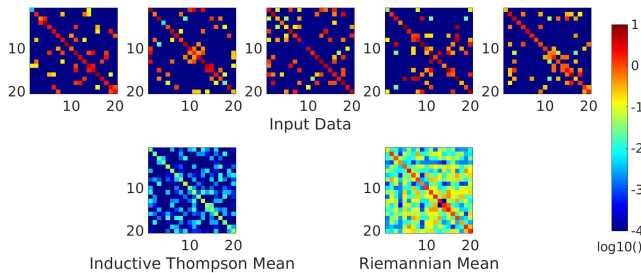


Fig. 5. The inductive Thompson mean and Riemannian mean for a set of 5 input data SPD matrices with distinct sparsity patterns.

Corollary 5. (Sparsity preservation II). If $\{Y_1, \dots, Y_k\} \subset \mathbb{S}_{++}^n$ is a set of sparse SPD matrices with $k \ll n^2$, then $M(Y_1, \dots, Y_k)$ is sparse.

Figure 4 shows the inductive Thompson mean and Riemannian mean of 5 input data matrices with the same sparsity pattern, showing how the inductive Thompson mean preserves the sparsity pattern whereas the Riemannian mean corrupts it. Figure 5 shows the results of the corresponding simulations for a second set of 5 sparse input matrices with distinct sparsity patterns.

REFERENCES

Afsari, B. (2011). Riemannian L^p center of mass: Existence, uniqueness, and convexity. *Proceedings of the American Mathematical Society*, 139(2), 655–673.

Alexander, D., Seunarine, K., Nedjati-Gilani, S., Hall, M., Parker, G., Bai, Y., and Cook, P. (2006). Camino: Open-source diffusion-MRI reconstruction and processing. In

Proceedings of the 14th Scientific Meeting of the International Society for Magnetic Resonance in Medicine (ISMRM), Seattle, WA, USA.

Arsigny, V., Fillard, P., Pennec, X., and Ayache, N. (2006). Log-Euclidean metrics for fast and simple calculus on diffusion tensors. *Magnetic Resonance in Medicine*, 56(2), 411–421. doi:10.1002/mrm.20965.

Barachant, A., Bonnet, S., Congedo, M., and Jutten, C. (2012). Multiclass brain-computer interface classification by Riemannian geometry. *IEEE Transactions on Biomedical Engineering*, 59(4), 920–928. doi:10.1109/TBME.2011.2172210.

Basser, P.J., Mattiello, J., and LeBihan, D. (1994). MR diffusion tensor spectroscopy and imaging. *Biophysical journal*, 66(1), 259–267.

Mostajeran, C., Da Costa, N., Van Goffrier, G., and Sepulchre, R. (2024). Differential geometry with extreme eigenvalues in the positive semidefinite cone. *SIAM Journal on Matrix Analysis and Applications*, 45(2), 1089–1113. doi:10.1137/23M1563906.

Mostajeran, C., Grussler, C., and Sepulchre, R. (2020). Geometric matrix midranges. *SIAM Journal on Matrix Analysis and Applications*, 41(3), 1347–1368. doi:10.1137/19M1273475.

Nussbaum, R.D. (1994). Finsler structures for the part metric and Hilbert’s projective metric and applications to ordinary differential equations. *Differential Integral Equations*, 7(5-6), 1649–1707.

Pennec, X., Fillard, P., and Ayache, N. (2006). A Riemannian framework for tensor computing. *International Journal of Computer Vision*, 66(1), 41–66. doi:10.1007/s11263-005-3222-z.

Said, S., Bombrun, L., Berthoumieu, Y., and Manton, J.H. (2017). Riemannian gaussian distributions on the space of symmetric positive definite matrices. *IEEE Transactions on Information Theory*, 63(4), 2153–2170. doi:10.1109/TIT.2017.2653803.

Thompson, A.C. (1963). On certain contraction mappings in a partially ordered vector space. *Proceedings of the American Mathematical Society*, 14(3), 438–443.

Van Goffrier, G.W., Mostajeran, C., and Sepulchre, R. (2021). Inductive geometric matrix midranges. *IFAC-PapersOnLine*, 54(9), 584–589. doi:10.1016/j.ifacol.2021.06.120. 24th International Symposium on Mathematical Theory of Networks and Systems MTNS 2020.